1 of

NASA TECHNICAL TRANSLATION

NASA TT F-14,154

TRANSONIC TESTING OF THE ENGINE NACELLE AIR INTAKE AND AFTERBODY

J. Leynaert

Translation of: "Entrée d'air et arrière-corps de fuseau-moteur en transsonique", Office National d'Etudes et de Recherches Aerospatiales, Chantillon, France, ONERA-TP-943, 1971, 11 pages.

NATIONAL AERONAUTICS AND SPACE ADMINISTRATION
WASHINGTON, D.C. 20546 MARCH 1972

TRANSONIC TESTING OF THE ENGINE NACELLE AIR INTAKE AND AFTERBODY

Jacky Leynaert*

ABSTRACT. An example is presented of the study of a double-flux engine nacelle at high subsonic Mach numbers. The investigation was carried out at high Reynolds numbers with two separate models for the air intake and the afterbody.

The test on the afterbody shows that the conditions of variable jets do not significantly affect the upstream flow around the nacelle intake and cowl, except for the immediate vicinity of the exhaust. This fact justifies the large scale study of the air intake with a model supported downstream by a cylindrical tube replacing the jet.

In the same way, mass flow rate variations of the air intake do not influence the flow around the afterbody, within given limits. This makes it possible to study the afterbody on an upstream sting.

The significance and limitations of these studies are discussed according to the test results.

1. Wind Tunnel Study of Aircraft with Engines

Wind tunnel study of aircraft drag, as opposed to conventional engine /13-2** thrust, is usually performed by testing a model fitted with hollow nacelles through which a certain "natural" mass flow passes. This can be adjusted in the transonic regime to give a mass flow representative of the real engine by

---

*Division Chief, "Internal Aerodynamics".

**Numbers in the margin indicate the pagination in the original foreign text.

diverting an appropriate amount through internal ducting.

If the drag of the conventional internal flow is subtracted from the value of the total force on the model under these conditions, a certain external drag is obtained.

In the case of real operation with an engine, this drag must then be corrected to take into account the differences in interaction between the internal and external flows at the nacelle exhaust.

For example, one method consists of closing off the air intake with a profiled ogive and feeding the pod with compressed air from inside the model, so that the axial reaction is known (or zero). Two series of tests are then carried out: one with simulation of the real jet, the other with simulation of the "natural" jet from the hollow nacelle. The difference of the measured forces is recorded, with a deduction made for the ideal thrusts of the jets. It seems that at present this technique would be most satisfactory if it were reserved for testing with a "motorized pod" and for fixed characteristics [1]. This is extremely expensive.

Having thus established the overall elements for propulsion evaluation in a given configuration and for a more comprehensive study of possible improvements, it is useful to determine the portion of the drag arising from the air intake, from the afterbody of the engine pod, and from interactions between the nacelle and the other parts of the aircraft, respectively.

To obtain these results at Reynolds numbers as realistic as possible, special mounting systems are used:

— The air intake is placed in the wind tunnel ahead of a tubular support held at the downstream end, which allows extraction and precise measurement of the mass flow.

— The afterbody is mounted on an upstream sting which is fed with compressed air and may carry an element of the nacelle suspension pylon [2].

The forces on the air intake and the afterbody are measured via internal balances or deduced from the pressure distributions. These two types of tests allow the proper drag of the engine pod to be determined.

— The interaction drag can be obtained by comparison of the drag of the complete model (corrected for the effect of the jet) and the sum of the drag of the aircraft model without nacelle plus the proper drag of the pod.

We propose to discuss some special points of this analytical technique in the following sections.

2. Isolated Engine Pod — Independence of Tests on Air Intake and on Afterbody

The discussion will be limited to the study of the drag proper of the engine pod. This is deduced, as has been said, from separate studies of the air intake and of the afterbody. The problem is to simulate as exactly as possible in each test the in-flight conditions of flow around the corresponding part of the real engine pod, assumed to be isolated.

Air intakes of present classical configurations do not present any difficulty, as tests show that there is no appreciable effect of jets — or of the shape of the extreme downstream portion of the afterbody on the flow farther upstream — on the fairing. Figure 1 is quite significant in this respect. It gives pressures measured on the downstream portion of the fairing for several rates of expansion of the annular jets of a double-flux engine simulated in a wind tunnel. These pressures are rigorously invariant out to about a half-radius of the principal exhaust section. This result thus justifies mountings for intake studies in which the afterbody is replaced by a simple sting.

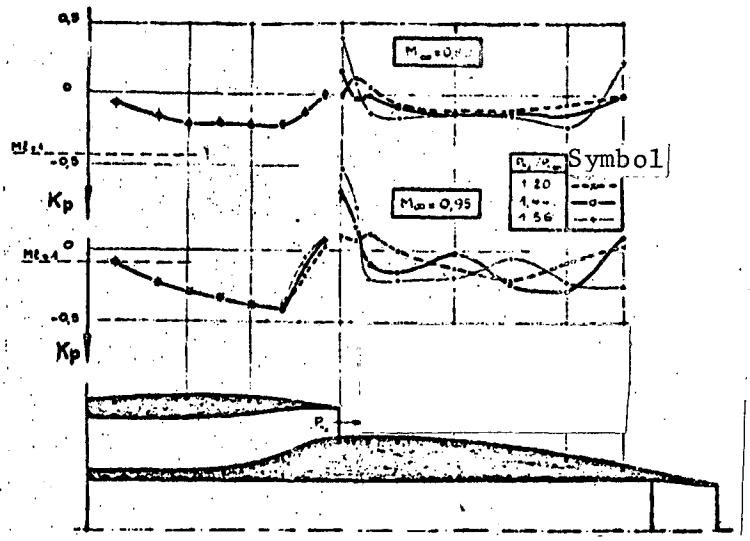

Figure 1. Measurement of pressures on the fairing for variable jet pressures.

The problem is more difficult for the afterbody.

Summaries of pressures on an engine-pod fairing taken during a test of an air intake held by a downstream sting are shown in Figures 2 and 3. The figures show that at the different Mach numbers considered, the downstream flow is only slightly affected by the variations in the mass flow at the intake, over a rather wide range of adjustment.

The curves deserve some comments, however.

— At $M_\infty = 0.8$, the unperturbed downstream region extends over the major portion of the fairing, even at the smallest mass flow coefficient shown, $\varepsilon = A_\infty/A_1 = 0.40$.

— At $M_\infty = 0.85$ and at reduced mass flow ($\varepsilon < 0.69$), the region of influence of the supersonic effect of surrounding the inlet lip extends further

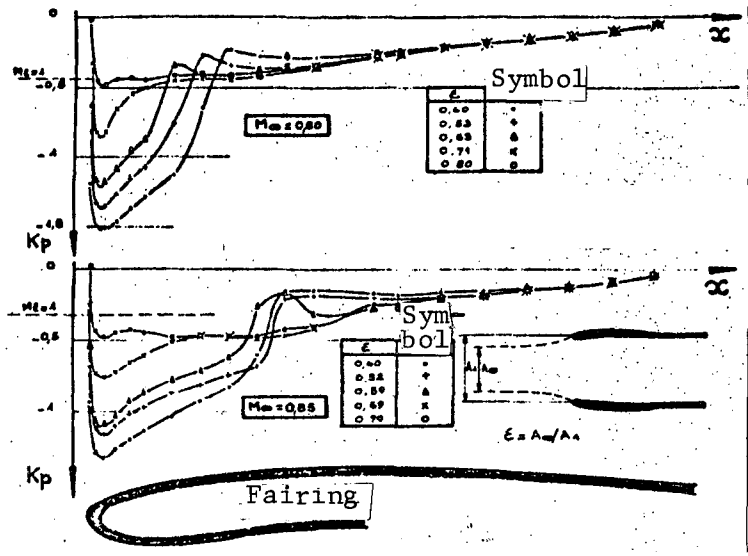

Figure 2. Effect of mass flow coefficient

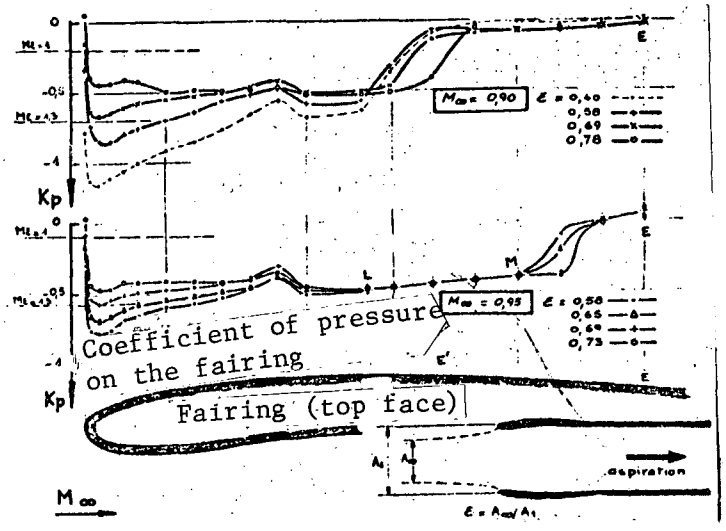

Figure 3. Effect of mass flow coefficient.

downstream on the fairing, but is still rather limited. No effect can be seen downstream of a certain abscissa for $\varepsilon > 0.46$; a slight drift of the pressure coefficients occurs when the mass flow coefficient falls below this value.

— At $M_\infty = 0.90$, the supersonic zone extends farther. Only a small subsonic region near the aft end of the fairing remains uninfluenced by the effects upstream, except for mass flow

coefficients of 0.40 or less, where a small change appears.

A certain pressure stabilization in the supersonic zone does, however, /13-3
begin to appear around the maximum diameter.

— At $M_\infty = 0.95$, this stabilization has been perfectly established. It can be noted that at this Mach number a large portion LM of the supersonic zone remains invariant over the different mass flow coefficients studied. It can apparently be assumed that in this case, variations in the mass flow at the air intake now affect the downstream flow only through the boundary layers, to which one can impute the slight displacements of the shock wave which limit the supersonic zone, and which leave the downstream subsonic flow practically unchanged.

Finally, it can be seen in every case that, except for boundary-layer effects, there is a certain downstream region unperturbed by fairly large variations in mass flow, including configurations in which the supersonic effect of surrounding the leading edge of the fairing produces a large increase in drag, as we shall see. The extent of the upstream domain which is sensitive to variations in the mass flow seems rather curiously to pass through a maximum at a Mach number of about 0.9, for the present example.

We can conclude from these remarks that a match between separate tests of the air intake and the afterbody will be assured if it is possible to define a mounting for the latter such that the invariant portion of the pressure distribution to be studied will be faithfully reproduced there. In making this match, it is, however, necessary to take the secondary effects of the boundary layers into consideration.

3. Pressures Compared for the Two Test Mounts of the Air Intake and the Afterbody

Figure 4 presents a first trial match of separate tests of the air intake

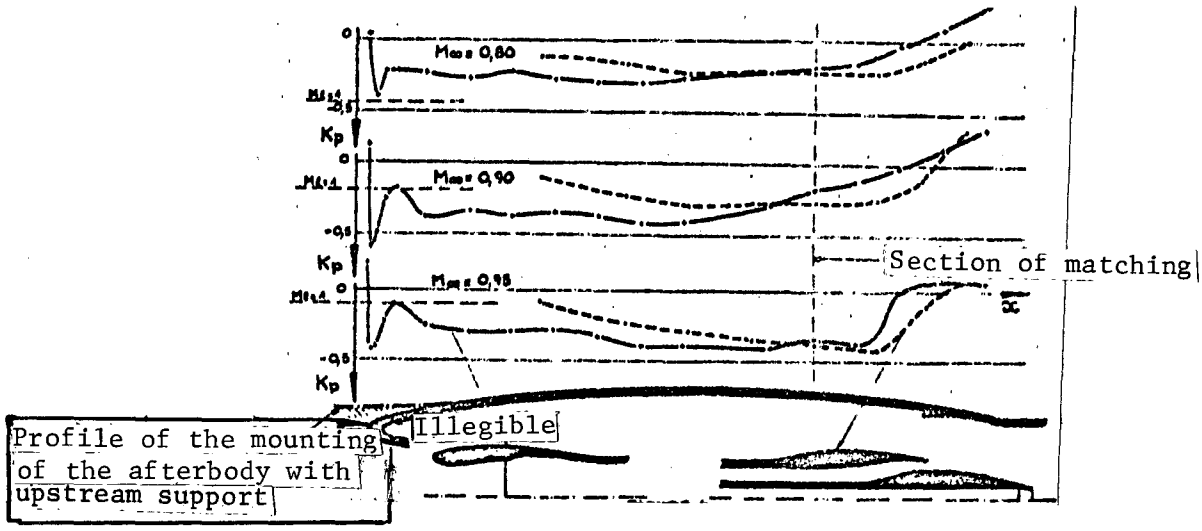

Figure 4. Pressure coefficients on an afterbody held upstream, and on an air intake held downstream.

and the afterbody. There are unacceptable differences in the downstream zone where there should be agreement.

These differences have been attributed [3] to the very rudimentary representation of the upstream flow by the sting, which has a diameter clearly larger than that of the stream tube which normally passes through the air intake. To test this hypothesis, a calculation of the theoretical pressure distributions was carried out for the two configurations, assuming incompressibility (rheoelectric analog).

The theoretical results of Figure 5 show clearly the lack of agreement with tests in the upstream portion, but have no effect on the pressure distribution in the downstream part where the condition for matching was investigated.

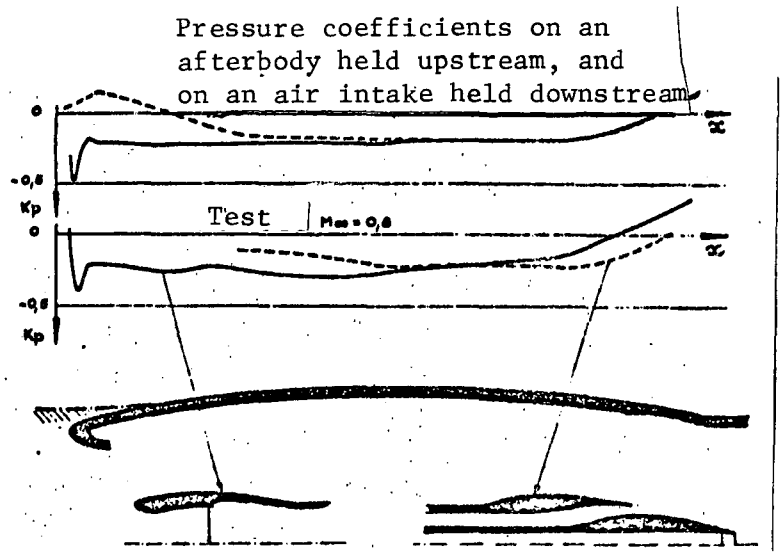

Figure 5. Pressure coefficients on an afterbody held upstream, and on an air intake held downstream.

Another cause of disagreement could be a difference in boundary-layer thickness, although the effect of this parameter should be rather marked when shock recompressions occur, which is not the case for the downstream flow at the Mach number considered here (M = 0.8).

A slightly more complex test mount has been designed to eliminate these two sources of error (Figure 6). This mount includes an upstream sting of the same diameter as the average stream tube captured by the air intake, and permits a more correct representation of the leading-edge profile, as well as a certain mass flow of aspiration of the boundary layers of the sting, just under this leading edge.

This configuration has been studied by a rheo-electric analog, and theoretically should produce a very correct restoration of the flow field (Figure 6).

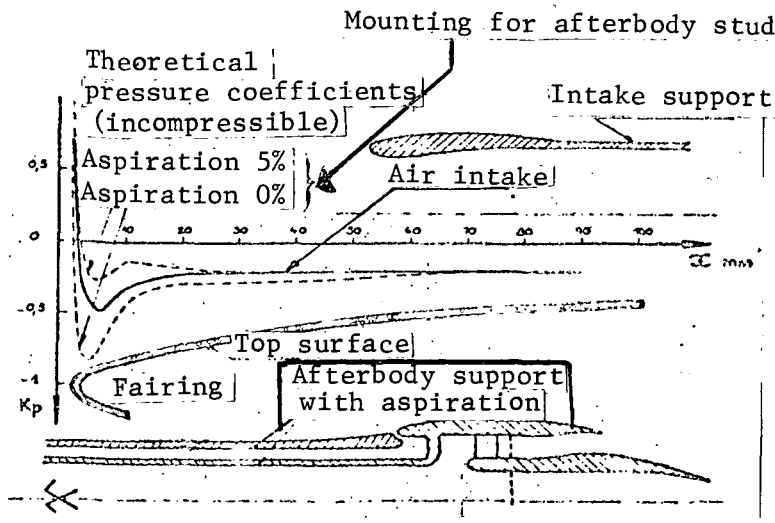

Figure 6. Mounting of afterbody by upstream support with aspiration at the inlet.

The last possible cause of disagreement, and without doubt the most important, results from unfavorable experimental conditions (very high levels of obstruction, different wind tunnels for the two types of test) (see Figure 7).

4. Significance of the Air-Intake Drag Coefficients

It is now of interest to define and discuss the terms of the drag evaluation which can be determined with the assistance of the mountings defined above.

For this, we refer to a hypothetical ideal configuration such that the mass flows delivered by the nozzles expand isentropically out to ambient pressure p_∞, and such that the exterior flow at the surface formed by the captured stream tube ∞ I (Figure 8), the external profile of the fairing IEB, and the downstream stream tube limiting the jet of the ideal nozzle B-∞ is free of all irreversibility due to shocks or viscosity.

In this configuration, the axial resultant of the relative pressure forces $(p - p_\infty)$ on the contour (assumed to be solid) ∞ IEB -∞ — which would represent the conventional drag of an engine pod — is zero.

The net pressure drag of the air intake up to section E (chosen for matching the separate studies of intake and exhaust) will be defined for a given internal

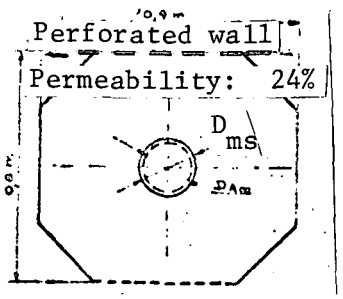

Figure 7. Intake test,

Wind tunnel S_3ch

D (major section) = 195.3 mm

D (stream tube) = 169 mm

$$\frac{A_{ms} - A_\infty}{A_{tunnel} - A_\infty} = 2\%$$

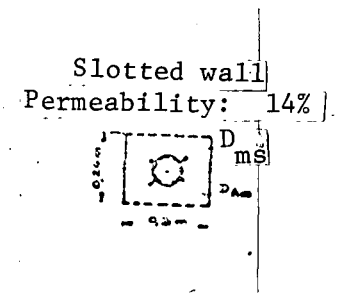

Afterbody test,

Wind tunnel S_3ch

D (major section) = 97.4 mm

D (stream tube) = 90 mm

$$\frac{A_{ms} - A_\infty}{A_{tunnel} - A_\infty} = 1.7\%$$

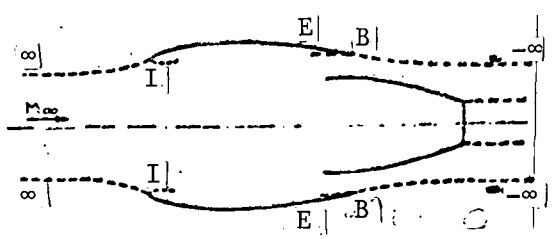

Figure 8

mass flow, by the difference between the pressure drag for the case studied and that for the preceding ideal case over a contour ∞ IE with the same mass flow. In particular, if the air-intake configuration contains a cylindrical profile downstream from section E, the drag up to that section is zero in ideal flow, and the axial resultant of the relative pressure forces over the contour ∞ IE gives the net pressure drag directly.

The net pressure drag thus defined would be of absolute importance only if the effective pressures downstream from section E would exactly match those of the ideal configuration.

Strictly speaking, this match does not exist, and there is an interaction between the fore- and afterbodies. The preceding hypothetical construction defined from the net intake drag is thus purely conventional. However, it is justified in practice by the observations of Section 2 concerning mounts for air-intake studies. It is thus seen that at moderate subsonic Mach numbers, with mass flows sufficiently high to prevent an irregular surrounding of the /13-4 leading edge, the downstream pressures are not effectively changed by variations in mass flow.

At Mach numbers of 0.8 or more, it is impossible to avoid a supersonic surrounding of the leading edge, even in the most favorable case of maximum mass flow: The preceding definition seems to lose all theoretical significance.

However, comparison of pressures at different Mach numbers (Figure 9) shows that they remain practically invariant up to M = 0.85. It can thus be assumed that the flow downstream remains rather close to the "ideal" flow, so that the proposed definition still has a practical meaning. On the other hand, above M = 0.9, although the flow toward the after portion of the fairing appears to become regular again and to be insensitive to appreciable variations in the mass flow, the pressure coefficients differ more and more from those obtained at smaller Mach numbers. Under these conditions, it can be assumed that the idea of net pressure drag by itself no longer reflects the effect of the air intake on the pressure drag of the whole pod.

5. Friction and Boundary Layer

The net pressure drag of the air intake represents the sum of the drag of the wave produced by any shock which may occur on the profile, plus the drag due to effects of boundary-layer displacement.

This pressure drag must be complemented by the friction drag to obtain the net drag of the air intake.

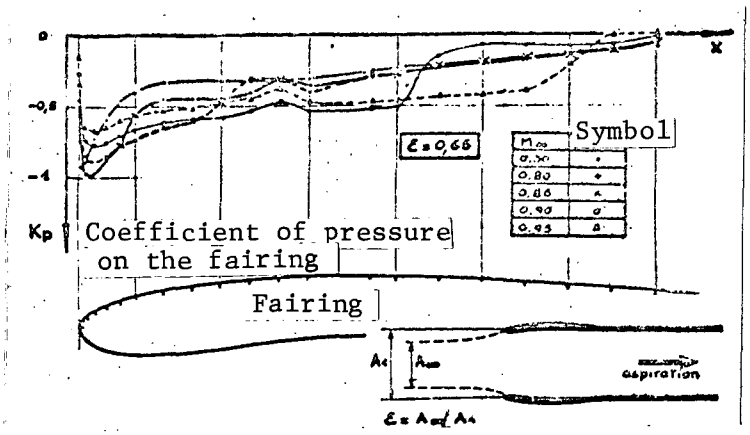

Figure 9. Effect of Mach number.

The presence of boundary layers at the junction-section obviously affects the absolute character of the net intake drag, since these boundary layers play a considerable role in the flow at right angles to the afterbody. It is thus necessary to restore the state of these boundary layers properly in testing the isolated afterbody to determine the total drag as the sum of the net drags of the intake and the afterbody measured separately.

6. Estimating the Pressure Drag of an "Ideal" Configuration (for reference)

The air-intake test and the experimental measurements described in the following section allow one to obtain the axial resultant X_p of the pressures on the contour ∞ IE of Figure 8, or the pressure drag. As shown in Section 4, to obtain the net pressure drag, it is necessary to subtract from it the pressure drag $\overline{X}_p$ corresponding to an "ideal" exterior flow: i.e., with neither shock nor viscosity and with the same mass flow. In the particular case of a cylindrical fairing downstream from E, $\overline{X}_p$ is zero. In the general case, $\overline{X}_p$ could be obtained by a calculation for perfect fluid flow.

Experimentally, if, in the general case, one has available a test at a moderate subsonic Mach number with a mass flow coefficient large enough that the external flow has no shock wave, the integral of the pressures over the contour ∞ IE, deduced from the measurements, is a first approximation to $\overline{X}_p$.

The following remark permits a more exact value to be obtained, however,

Outside the boundary layer, the flow is identical to the flow of a perfect fluid around the profile of the fairing enlarged by the displacement thickness δ^*.

The integral of the pressures applied to the stream tube ∞ I ... C* is written, to the second order (see Appendix):

$$\int_{\infty I E^*} (p - p_\infty)\,\pi\, \frac{d(R+\delta^* \cos\theta)^2}{ds}\, ds = \int_{\infty I E} (p - p_\infty)\,\pi\, \frac{dR^2}{ds}\, ds + \int_{\widehat{IE}} (p - p_\infty)\,2\pi\, \frac{d(R\delta^* \cos\theta)}{ds}\, ds$$

When the fairing is cylindrical downstream from E, the first integral is zero, according to d'Alembert's Theorem. Consequently, in this particular case, $\overline{X}_p$, which is also zero, is equal to the sum of X_p, represented by the second integral, and the third term.

In the general case, where the fairing has a slight slope downstream from E, we assume a priori that the relation

$$\overline{X}_p = X_p + \int_{\widehat{IE}} (p - p_\infty)\,2\pi\, \frac{d(R\delta^* \cos\theta)}{ds}\, ds$$

is still valid for an approximate calculation of $\overline{X}_p$.

The evaluation of δ^* along the profile, and the measurements of $p - p_\infty$ which are necessary for calculation of the correction term, are part of the experimental process described below.

7. Techniques for Measuring Air-Intake Drag

The drag of an air intake can be decomposed into three terms:

X_a : additive drag, the axial resultant of the effects of pressure on the meridian stream tube (∞ I)

$X_{p_{IE}}$: pressure drag on the external fairing IE

X_f : friction drag on the external fairing IE

$X = X_a + X_{p_{IE}} + X_f$

Three methods of measuring X will be rapidly called to mind: /13-5

(a) The mass flow (i.e., the stream tube at infinity upstream) being known, a measurement of the stagnation pressure of the subsonic flow around the downstream sting, within a zone where the static pressure has again become uniform and equal to p_∞, allows the value of the drag X to be obtained by application of the momentum theorem between infinity upstream and the plane of measurement.

(b) A second method consists of weighing, with an internal balance, an element of the air intake consisting of the external profile (C) out to the section of match E and the internal profile out to a section where the relative internal dynalpy $D_S = \int_A (p - p_\infty)\, dA + \ldots\, dq_m$ can be measured conveniently.

dA : element of normal area

u : axial velocity component

dq_m : elementary mass flow

From the balance readings, one may deduce X_b, since $X_b = X_{p_{IE}} + X_f + X_{int}$, where X_{int} represents the axial force exerted by the flow (pressure and friction) on the weighed internal portion of the fairing.

A second relation is supplied by the measurement of D_S and the momentum evaluation:

$$D_S - q_m V_\infty = X_a - X_{int}$$

from which we have $$X = X_{p_{IE}} + X_f + X_a = X_b + D_S - q_m V_\infty$$

(c) If one does not have an overall measurement from a balance, but does have measurements of pressure on the fairing (external and internal) which permit integration of the axial pressure forces, plus measurements of the external and internal boundary layers which allow the friction to be evaluated as shown below, one can calculate from these measurements the resultant $X_{p_{IE}} + X_{int}$, then $X_{p_{IE}} + X_a$ by the relation

$$X_{p_{IE}} + X_a = X_{p_{IE}} + X_{int} + D_S - q_m V_\infty$$

and X by $$X = X_{p_{IE}} + X_a + X_f.$$

It is by this last method that the curves of pressure drag ($X_a + X_{p_{IE}}$) shown in Figure 10 have been obtained, at different Mach numbers for the configuration whose pressure distributions have been presented previously.

At a Mach number of 0.8 or more, the curves show a very marked knee in the drag when the mass flow coefficient decreases below a certain value. At a Mach number of 0.5, this knee does not appear in the range of mass flow coefficients studied. An examination of the pressure-distribution curves seems to show that this knee in the drag corresponds to a focusing of compression waves, which close the external supersonic zone around the leading edge — the supersonic recompression being more spread out for a large mass flow coefficient — while a strong shock wave is formed and stabilized a little nearer the leading edge when the mass flow coefficient is reduced.

The friction drag X_f has been deduced from a measurement of the external boundary layer on the downstream part of the fairing.

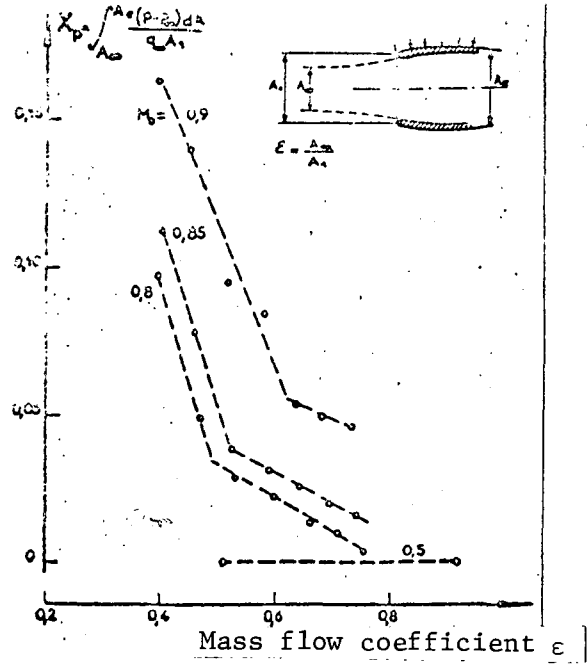

Figure 10. Pressure-drag coefficient.

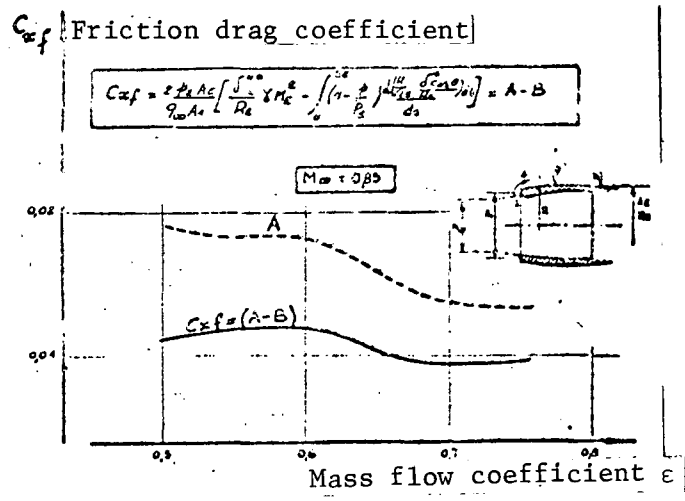

Figure 11

However, as the profile is curved inward, the results of this measurement are not sufficient for determining the friction: it is necessary to make a correction to include the effect of boundary-layer displacement. This calculation, given in detail in the Appendix, leads to the following expression:

$$X_f = \pi R_E r_E \gamma M_E^2 \Gamma_E^{**} - \int_{\overline{ES}} (r_E - r) \pi \frac{d(\rho r^2 \cos\theta)}{ds} ds$$

in which the index E represents the quantities evaluated at E (at the edge of the boundary layer), and s represents the arc of the exterior profile of the fairing:

δ_E^{**} is the measured momentum thickness at E;

$\delta^*(s)$ is obtained by calculation of the boundary layer, possibly adjusted to agree with the experimental value of δ^* at E.

The second term is not negligible with respect to the first; in the example of Figure 11, their ratio is of the order of 50%. When boundary layer detachment appears around the leading edge, classical calculation obviously becomes quite imprecise, considering the uncertainty in δ^* and the inexactness of the hypothesis of constant static pressure within the thickness of the boundary layer in this region.

It is interesting to compare this formula to that giving the boundary layer correction in the experimental study of an "ideal" configuration. If it is assumed that $p_E = p_\infty$, it is found that the ideal drag is equal to the real drag less the friction drag calculated at E by the "cylinder or flat plate" formula.

8. Drag of the Afterbody

The afterbody drag is to be discussed in the same manner as the intake drag, to which it is complementary.

It can be obtained experimentally by comparison of the thrust of an ideal afterbody with the thrust of a real afterbody, measured by a balance weighing the sum of forces on the external fairing downstream from the match-section E and the internal reaction of the jet [3].

9. Conclusion

/13-6

Different considerations and a rather complete example of the analysis of flow around the fairing of an engine pod have allowed the principles of the study of the drag of an engine pod and its elements to be defined. In particular, the conditions under which the behavior of the air intake and the afterbody can be studied on separate models in a wind tunnel have been investigated. It is justified to study the intake on a model supported by a downstream sting, and it seems possible (with certain reservations concerning the mass flow collected)

to study the flow on the afterbody with a model with an upstream sting. However, a deeper study of this last device is needed to demonstrate this possibility in practice.

REFERENCES

1. Kutney, John T. Airframe Propulsion System Integration Analysis Using the Propulsion Simulation Technique. AGARD CP, No. 71 on Aerodynamic Interference.

2. Holdhusen, James S. Analysis and Demonstrations Techniques for Installation Aerodynamics Effects on High By-Pass Turbofan. AGARD CP, No. 34. Thirty-second meeting of the Prop. & Energetics Panel of AGARD-TOULOUSE 9-13.9.1968.

3. Engine Airplane Interference in Transonic Tests. AGARDograph (in press).

APPENDIX

/13-7

EVALUATION OF THE EXTERNAL FRICTION DRAG OF AN AIR INTAKE

We shall consider an axisymmetric air intake placed in a flow (p_∞, ρ_∞, V_∞) and collecting a well-defined internal mass flow. Let I be the stagnation point of this flow, and (C) the contour of the external fairing downstream from I. By (C*) we denote the contour obtained by adding at each point (s) of (C) the local displacement thickness of the boundary layer $\delta^*(s)$.

It is known that beyond the edge of the boundary layer (δ), the real flow around (C) is identical to perfect-fluid flow defined by the contour (C*). In particular, these two flows have in common the border streamline PI, and at every abscissa s the pressures are identical on (C) and (C*).

This being assumed, let E be the downstream extremity of the weighed part of the fairing, and E E* E' R be a normal to the wall at E, assumed to be identical to the normal to the axis. QR designates a streamline sufficiently far from the axis so that we can apply the momentum theorem in projection on the axis — first to a closed test surface defined by I E R Q P I in the real flow, then to E* R Q P I in the perfect-fluid flow around (C*). Thus, we obtain the two expressions:

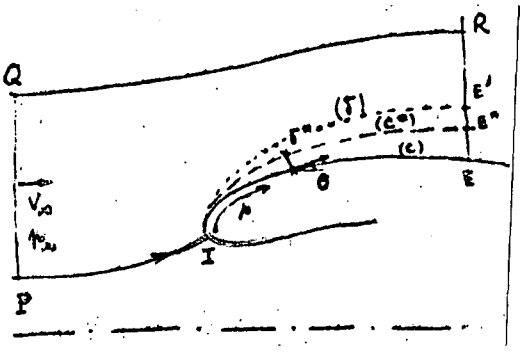

$$X_f + \int_{(IE)} (p - p_\infty)\, dA + \int_{(ERQPI)} [(p - p_\infty)\, dA + u\, dq_m] = 0 \qquad (1)$$

$$\int_{(IE^*)} (p - p_\infty)\, dA + \int_{(E^*RQPI)} [(p - p_\infty)\, dA + u\, dq_m] = 0 \qquad (2)$$

In these expressions: dA designates the projection normal to the axis of an element of area;

u is the axial component of the velocity;

dq_m is the mass flow leaving the contour element considered.

If (2) is subtracted from (1), we have, taking into consideration the common parts of the last integrals

$$X_f + \int_{(IE)} (p - p_\infty)\, dA - \int_{(IE^*)} (p - p_\infty)\, dA + \int_{EE'} [(p - p_\infty)\, dA + u\, dq_m] - \int_{(E^*E')} [(p - p_\infty)\, dA + u\, dq_m] = 0 \qquad (3)$$

But, given that at the same curvilinear abscissa s, $p - p_\infty$ is identical on (C) and (C*), and that on (C), $dA = d(\pi R^2)$ and on (C*), $dA = d[\pi(R + \delta^* \cos\theta)^2]$ (slope of the profile is $\tan\theta$), the first two integrals can then be written to the second order in δ^*, assuming a small slope at E ($\cos\theta_E \simeq 0$):

$$\int_{(IE)} (p - p_\infty)\, dA - \int_{(IE^*)} (p - p_\infty)\, dA = -\int_{IE} (p - p_\infty)\, 2\pi \frac{d(R\delta^* \cos\theta)}{ds}\, ds \qquad (4)$$

Furthermore, the last two integrals can be written, according to the Prandtl hypothesis, as

$$(p_E - p_\infty)\, 2\pi R_E \delta_E^* + \int_0^{\delta_E} 2\pi R_E (\rho u^2 - \rho_e u_e^2)\, dy + 2\pi R_E \rho_e u_e^2 \delta_E^* \qquad (5)$$

where ρ_e and u_e designate values at E in the ideal flow around (C*) — i.e., also in the real flow at the border of (δ).

Now, from the classical definitions of δ^* and δ^{**} (momentum thickness), one has identically

$$\int_0^{\delta_E} (\rho_e u_e^2 - \rho u^2)\, dy = \rho_e u_e^2 (\delta_E^* + \delta_E^{**}) \qquad (6)$$